Reactivity of coronene with O-atoms, a possible route to ketene in the interstellar medium

Francois Dulieu, Sabine Morisset, Abdi-Salam Ibrahim Mohamed, Leon Boshman, Stephanie Cazaux, Dominique Teillet-Billy, Saoud Baouche, Nathalie Rougeau

Version of Record: https://www.sciencedirect.com/science/article/pii/S2405675819300132
Manuscript_bf9b52cc874d920dd9a5973863dca699

Reactivity of coronene with O-atoms, a possible route to ketene in the interstellar medium

Francois Dulieu[a,1], Sabine Morisset[c], Abdi-Salam Ibrahim Mohamed[a], Leon Boshman[d,f], Stephanie Cazaux[b,e], Dominique Teillet-Billy[c], Saoud Baouche[a], Nathalie Rougeau[c]

[a] *Université de Cergy-Pontoise, Sorbonne Université, Observatoire de Paris, PSL University, CNRS, LERMA, F-95000, Cergy-Pontoise, France*
[b] *Delft, The Netherlands*
[c] *Institut des Sciences Molculaires d'Orsay, ISMO, CNRS, Université Paris-Sud, Université Paris Saclay, F-91405 Orsay, France*
[d] *Kapteyn Astronomical Insitute, Groningen, The Netherlands*
[e] *University of Leiden, P.O. Box 9513, 2300 RA, Leiden, The Netherlands*
[f] *Zernike Institute for Advanced Materials, University of Groningen, Nijenborgh 4, 9747AG Groningen, The Netherlands*

Abstract

PAHs are one of the important components of the carbonaceous matter of the Universe. They are not detected in the darkest regions of the Interstellar Medium and one possible reason could be their chemical transformation through gas phase reactions. In particular, their oxidation was considered ineffective because the reaction barriers appear to be too high, based on combustion studies conducted at high temperatures. For the first time, we experimentally studied the oxidation of Coronene, a PAH archetype, at low temperature (50 K), as well as the oxidation of hydrogenated Coronenes. It appears that reactivity is higher than expected and that the fragmentation of coronene is a significant channel of the oxidation. Furthermore, hydrogenated coronenes are very reactive to oxygen. To understand the experimental data, DFT calculations were performed. They confirm a low oxidation barrier (0.11 eV) and show that oxygen is preferentially inserted at the periphery of the coronene and propose a reaction mechanism for fragmentation also involving a hydrogen atom. An estimate of the orders of magnitude shows that PAH oxidation may explain

[☆] Fully documented templates are available in the elsarticle package on CTAN.

part of the decrease in their abundances in warm environments.

Keywords: ISM, PAH, Oxygen reactivity, Fragmentation

1. Introduction

The interstellar medium (ISM) is chemically complex, and is the result of the interplay between gas and solid particles such as dust grains or polycyclic aromatic hydrocarbons (PAHs)(Allamandola et al., 1989). PAHs represent a carbon reservoir, accounting for about 10% of the galactic carbon budget (Tielens, 2013), and have the largest geometric surface area over the grain distribution (Weingartner and Draine, 2001). Because of this high surface area, PAHs can be important interstellar catalysts for the formation of H_2 (Habart et al. 2004; Cazaux and Tielens 2004; Andrews et al. 2016; Castellanos et al. 2018) and are recognized to play an important role in the heating and the chemistry of these irradiated regions. In regions subject to UV photons, called photodominated regions (PDRs), PAHs are observed through Aromatic Infrared Bands (AIB)(Leger and Puget, 1984; Allamandola et al., 1985). The analysis of the mid-IR emission features suggests that they are produced by evaporation from very small grains (Rapacioli et al., 2005; Berné et al., 2007; Pilleri et al., 2015). In regions with higher extinction ($A_V \geq 2$) it is not clear whether PAHs exist and under which form. Some studies consider that PAHs condense on small grains (Jones et al., 2013; Köhler et al., 2015) or that PAHs are incorporated in the icy mantles covering dust particles (Bernstein et al., 1999; Gudipati and Allamandola, 2006; Bouwman et al., 2011). These PAHs embedded in water ices can undergo photochemical reactivity (Noble et al., 2017; Cuylle et al., 2014; Bernstein et al., 1999; Gudipati and Allamandola, 2003) and become oxygenated (Noble et al., 2017; Guennoun et al., 2010). Another possible explanation for the disappearance of PAHs could be their chemical transformation in the gas phase. Among the possible agents for the chemical transformation of PAHs are O atoms. O atoms are thought to remain in the gas phase at the edge of clouds for extinctions of Av$\simeq$3-5 (Hollenbach et al., 2009), and are thought to be locked

under the form of water ice at higher extinctions (Whittet et al., 2001). Understanding the interaction of the O atom and PAHs is the purpose of the study we are starting here.

The catalytic importance of PAHs has triggered numerous experimental studies to understand how PAHs interact with hydrogen atoms (Hirama et al. 2004; Thrower et al. 2012; Skov et al. 2016; Boschman et al. 2012; Cazaux et al. 2016). PAHs can easily become oxidized when present in water ices subjected to UV irradiation (Bernstein et al. 2002; Cook et al. 2015; de Barros et al. 2017; Noble et al. 2017; Guennoun et al. 2010). So far, only few experiments and theoretical calculations with O atoms have been reported , in the gas phase, on benzene (Boocock and Cvetanovic, 1961; Taatjes et al., 2010), naphthalene (Scapinello et al., 2015) and ethylene, C_2H_4 (Fu et al., 2012) as well as reaction with OH radicals on naphtalene (Ricca and Bauschlicher 2000) and antracene (Goulay et al., 2005). Theoretical studies (Fu et al. 2012; Nguyen et al. 2007; Taatjes et al. 2010; Scapinello et al. 2015) of O(^{3}P) reactions with ethylene, C_2H_4 (Fu et al. (2012)), benzene (Nguyen et al. (2007); Taatjes et al. (2010)) and naphthalene (Scapinello et al. (2015) have shown that, at low temperatures, these reactions proceed via an addition on a carbon atom, producing oxygenated species in triplet states. This first step is followed by H or H_2 elimination, isomerization or fragmentation of the oxygenated system. For the O(^{3}P) + C_2H_4 reaction, in the triplet states, the channels associated with the lowest energy barriers are the fragmentation into CH_2 + H_2CO and H elimination: H + CH_2CHO (Fu et al., 2012). The early experimental study of O + benzene reaction (Boocock and Cvetanovic, 1961) suggests isomerization to phenol or ring opening. More recent works have shown that H elimination is the dominant channel for the triplet states and that isomerization to phenol, in a singlet state, is obtained after inter-system crossing (spin change) (Barckholtz et al., 2001; Nguyen et al., 2007; Taatjes et al., 2010). Similar results have been obtained for the O + naphthalene reaction (Scapinello et al., 2015). All these works were developed in connection with combustion studies. In an astrophysical context, Ward et al. (Ward and Price, 2011) have studied oxy-

genation reactions of alkenes molecules, on a graphite surface, in the 12-90 K temperature range. They observed ethylene oxide and propene oxide formation above a surface temperature of 12 K. Using a kinetic model, they have shown that the barriers for the O + ethylene and O + propene reactions on the surface were an order of magnitude lower than the corresponding gas phase values. In their experimental study, Bernstein et al. have shown that oxidized species and partially hydrogenated species could be observed after UV irradiation of PAH's in water ice under astrophysical conditions (Bernstein et al., 1999). By studying photolysis of coronene in deuterated ices D_2O, these authors (Bernstein et al., 1999) also suggested that H atoms on oxygenated rings were more labile than H atoms on non oxygenated rings. Concerning the O/PAH reactions, the models used in astrophysics are based on combustion studies and imply in particular, high barriers to fragmentation (Wang and Frenklach, 1997; Appel et al., 2000). Thus, in these models, the interaction between atomic oxygen and PAHs is not involved in PAHs destruction. The objective of present experimental and theoretical work is to study O/PAH interactions and the influence of oxygenation on PAH destruction.

The document is organized as follows: in the first section, we present the experimental set-up and procedure. The second section presents the theoretical method. In the third section, our experimental and theoretical results are presented and discussed. In the last section, astrophysical implications are discussed.

2. Experimental procedure

The experiments were performed using the FORMOLISM (FORmation of MOLecules in the InterStellar Medium) setup, an ultra-high-vacuum chamber containing a quadrupole mass spectrometer (QMS) and a sample surface coupled to a cryostat (Congiu et al., 2012). The experimental configuration is sketched in figure 1. The sample surface consists of highly ordered pyrolytic graphite (HOPG) and the cryostat temperature can be kept constant at a set temperature

between 20 and 600 K.

Attached to this vacuum chamber is a retractable oven which is used to deposit pure coronene (≥ 99 %, Sigma-Aldrich) onto the surface. The oven, shown in the left of the figure, is heated to 420 K for gentle evaporation of coronene so that the molecules can be admitted in the chamber and be deposited on the cold finger. The HOPG surface is exposed to a beam from the coronene oven for a period of 15 minutes, at a surface temperature of 280 K. After exposure, the surface is annealed to 350 K in order to desorb the multilayers and only keep a monolayer of coronene following the same protocol as in (Thrower et al., 2012) with slight differences in the exposure and annealing temperatures. Two jet chambers are connected to the sample chamber. These two jet chambers can produce beams of atomic hydrogen and atomic oxygen by means of a microwave discharge source, and both beams are aligned at the center of the HOPG surface. These beams are presented in grey and red in the figure 1.

For the hydrogen beam, a degree of dissociation between 30% and 60% is established and measured each day, while this degree is approximately 15% for the oxygen beam. These dissociation efficiencies determine the amount of atomic versus molecular hydrogen (or atomic oxygen versus molecular oxygen) being deposited on the surface. Hydrogen deposition takes place at a surface temperature of 150 K and the exposure time varies between 2 and 4 hours depending on the degree of dissociation, so that the total hydrogen dose is constant. The equivalent exposed dose of hydrogen or fluence is about 7×10^{17} atoms/cm^2. If not stated, in the following, the temperature reported is the surface temperature. At 150 K, the sticking coefficient of H atoms is low (Cazaux et al. 2011; Chaabouni et al. 2012; Wakelam et al. 2017) and the residence time on a surface is extremely short. The surface temperature of 150 K prevents contamination with water during the hydrogenation phase, which could occur at lower temperatures. Oxygen exposure lasts for 15 minutes at a surface temperature of 50 K. The total fluence is 8×10^{14} atoms/cm^2, about or smaller than the surface density of adsorption sites of a solid surface (A monolayer, ML, is $\simeq 1\times10^{15}$ site/cm^2 (Ulbricht et al., 2002)). The 50 K temperature of the surface pre-

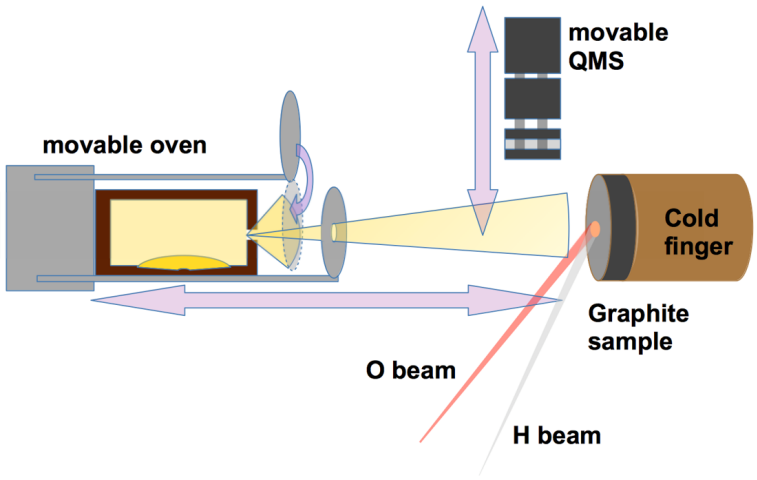

Figure 1: Experimental configuration. The movable oven containing coronene is placed at about 2 cm from the graphite sample (0.9cm in diameter) during the coronene deposition.In between depositions, the oven is retracted into its own vacuum chamber to maintain a low background pressure in the sample chamber. A diaphragm prevents PAH from being sprayed throughout the chamber. The oven can be opened and closed to control the deposition time. The O beam (pictured in red) and H beam (in light gray), are centered on the graphite sample. However, they do not cover the totality of the graphite, while the coronene film does. The QMS can intercept the beams, the exit of the PAH oven or be placed at 5 mm from the sample to perform the TPD. During deposition phases, it is moved backwards.

vents the formation of O_2 or O_3 (Minissale et al., 2016). The overlap of O and H beams covers around 40% of the coronene deposit. During the Temperature Programmed Desorption (TPD) measurement, the sample is heated up to 600 K at a rate of 18 K/min, while a quadrupole mass spectrometer tracks the evaporation of several masses from the surface. The heating phase is organized in two steps. From 50 to 200 K, which focuses mainly on volatile species (CO, CO_2, H_2O...), and in the 200-600K range where coronene associated species are targeted (discussed later).

We have performed four different types of TPD experiments:

- In the first experiment, a monolayer of coronene is deposited on the HOPG surface.
- In the second experiment, a monolayer of coronene is deposited and is subsequently exposed to a beam of atomic hydrogen (Coronene + H) at a surface temperature of 150 K.
- In the third experiment, a monolayer of coronene is deposited and is subsequently exposed to 1) a beam of atomic hydrogen and 2) a beam of atomic oxygen (Coronene + H + O).
- In the fourth experiment, a monolayer of coronene is deposited and is subsequently exposed to a beam of atomic oxygen (Coronene + O).

3. Theoretical calculations

The reactions of O(^{3}P) with coronene and with hydrogenated coronene in the gas phase, and the subsequent isomerization or fragmentation reactions have been studied within the Density Functional Theory (DFT) framework using the ADF code (te Velde et al. 2001; ADF2017 2017). Spin polarized calculations have been performed with the modified PW1K hybrid functional (Lynch et al., 2000) and with a $t\zeta p$ (triple zeta polarized) basis set of Slater type orbitals. Numerical convergence for geometry is obtained with gradients $< 10^{-3}$ Hartree per $\mathring{A}$ and distances are converged to 10^{-2} $\mathring{A}$. Numerical convergence for energies is 10^{-2} hartree. Transition states are obtained as stationary points on

the potential energy surface, and are characterized by an Hessian matrix with one negative eigenvalue associated with a motion along the reaction coordinate. For the different reactions considered, reaction energies and reaction barriers are defined as, for example for the oxygenation reaction :

$$\triangle E_{reaction} = E(C_{24}H_{12+n}O) - E(C_{24}H_{12+n}) - E(O(^3P)) \quad (1)$$

$$\triangle E_{barrier} = E(C_{24}H_{12+n}O^{\#}) - E(C_{24}H_{12+n}) - E(O(^3P)) \quad (2)$$

where $E(C_{24}H_{12+n}O)$ and $E(C_{24}H_{12+n}O^{\#})$ are the equilibrium and transition state energies of the oxygenated/hydrogenated species, respectively. n=0 and n>0 correspond to the coronene and to hydrogenated coronene, respectively. $E(O(^3P))$ is the atomic oxygen energy in the ground state. In the following, the energies are relative to the $C_{24}H_{12}$+$O(^3P)$ entrance channel.

The reactions between $O(^3P)$ and the coronene can proceed :

- on a triplet potential energy surface, thereby conserving the total spin,

- on a lower lying singlet potential energy surface, thereby including InterSystem Crossing (ISC) effects, i. e. couplings between molecular triplet and singlet states. Such ISC effects have been studied for the O + ethylene reaction (Fu et al., 2012) but remain challenging for more complex systems. In the present calculations, we consider only reactions on the triplet potential energy surface associated to the initial states of the reactants.

Previous DFT calculations on hydrogenation reactions of isolated coronene molecules deposited on a graphene surface have shown that hydrogenation energies in the deposited phase and in the gas phase are very similar, (with a maximum deviation of 10% (Morisset et al., 2017)). Indeed, coronene molecules are physisorbed on the graphene surface at a distance $d_{coronene-graphene} = 3.24$ Å. At such large distance, surface effects on the energy barriers for the hydrogenation reactions with H atoms coming from the gas phase are weak. In this case, the catalytic role of the surface is essentially to dissipate a fraction of the exothermicity and to stabilize products which could otherwise fragment or desorb. However, Ward and Price 2011 have shown that, on a graphite sample,

oxygenation barriers of alkenes are lowered by an order of magnitude. Indeed, in their experimental set-up, atomic oxygen and multilayers of alkenes were co-deposited at low temperatures. From the measurements of the reaction rates, they concluded that the barriers should be lower than in the gas phase. It is however not clear whether graphite/surface has an active role, or whether geometric constraints on alkene adsorption lower the barrier, as it is the case for NO hydrogenation on water ice (Nguyen et al., 2019). Moreover, the redistribution of the energy in a large ring compound such as coronene, is very different from that of a small alkene. Present experimental conditions are expected to be intermediate between the isolated molecule and multilayer cases of Ward and Price. Therefore in the present work, gas phase calculations represent upper limits values and are used as a basis for the interpretation of experimental results involving species deposited on a graphite surface.

4. Results & Discussions

In this section, the TPD spectra obtained for the four experiments: coronene, coronene + H, coronene + H + O and coronene + O are reported for the masses 300, 304, 305, 316 and 275. In addition, the gas phase DFT results are presented for the masses 316, and 275. These results are discussed in order to understand the oxidation process of the coronene and to propose a fragmentation channel.

4.1. Mass 300 : parent mass of coronene $C_{24}H_{12}$

In all the different experiments, coronene is first deposited on the graphitic surface held at 280 K and then flash heated up to 350 K before being cooled down to 250 K. The experimental TPD spectra for mass 300 amu for the four experiments are reported in figure 2. The coronene TPD spectrum has been plotted separately because it has been obtained in a slightly different measurement mode, during the preliminary tests of this study. For coronene, (figure 2a), the TPD spectrum shows a desorption peak located at a temperature of around 400 K. The line prolongating the desorption peak of the coronene intercepts

the temperature axis at approximately 360K. This value will be used later as a reference for the onset of the coronene desorption. The constant signal above 450 K is due to the contamination of the head of the QMS by the coronene. The spectra for the coronene + H, coronene + H + O and coronene + O are reported in figure 2b. The three spectra show nearly identical desorption peaks, with a maximum at $\sim$ 400 K. The small differences between 200 and 350 K are close to the noise level. Peak intensity comparison shows that the ratio of coronene molecules that have not reacted is approximately identical in the three experiments.

4.2. Mass 304 and 305: hydrogenated coronene $C_{24}H_{16}$ (+4H), $C_{24}H_{17}$ (+5H)

The spectra for the 3 different experiments for masses 304 and 305 amu are reported in figure 3a and 3b, respectively. These masses correspond to the addition of 4 and 5 hydrogen atoms on the coronene, respectively. Such hydrogenated species have already been detected in previous studies (Thrower et al., 2012). In the present work, the hydrogenation of the coronene is weak (a few % of coronene molecules are hydrogenated), and the hydrogenation degree is ranging from one to 8 extra H atoms. A total hydrogenation of the coronene molecules is not achieved because the H atom temperature is lower than 400 K, contrary to previous reported experiments where the temperature is $\sim$2000 K (Thrower et al., 2012, 2014). At lower temperatures, fewer barriers can be crossed (Jensen et al., 2019). This explains the lower efficiency in present experimental conditions. Therefore, in the present work, masses 304 and 305 are representative of hydrogenated coronene species with odd and even number of extra hydrogen, for which stabilities and reactivities are expected to differ. The intensity of the peak at mass 304 is greater than the one at mass 305. Indeed, species associated to mass 304 are closed shell species, which are created more rapidly than they are destroyed and are expected to have longer lifetimes on the surface. On the contrary, species associated to mass 305 are radical species, they are destroyed more rapidly than they are created and are expected to have shorter lifetimes (Cazaux et al., 2016). For the coronene + H experiment, the

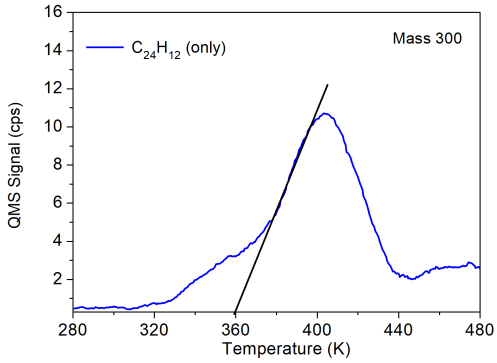

a)

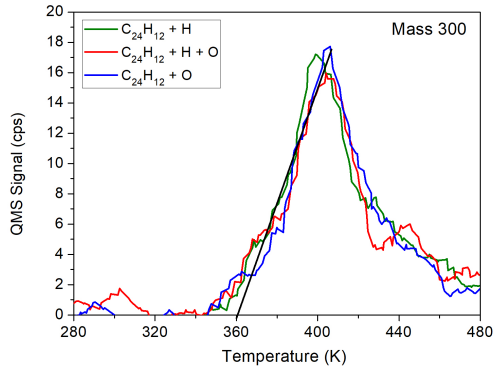

b)

Figure 2: TPD spectrum for mass 300 in the different experiments: (a) coronene only, (b) cororonene + H (green), cororonene + H + O (red) and coronene + O (blue). The black line represent the onset of the desorption of coronene which will be used for comparison with other masses.

TPD desorption peaks are located in the 310-390 K range, which is at lower temperatures than the desorption peak observed for coronene. This can be seen by comparing the slope of the desorption peak to the dashed line (corresponding the leading edge of the coronene desorption peaks).The desorption temperatures are related to the interaction energies (or adsorption energies) between the molecular species and the surface, the greater the interaction energy, the higher the desorption temperature. The interaction energies of isolated coronene or hydrogenated coronene molecules with a graphene surface have been calculated using the DFT method with a van der Waals functional accounting for long range interactions (Morisset et al., 2017). The adsorption energies obtained for the coronene and for the most stable fourth-hydrogenated coronene species, $C_{24}H_{16}$, are -1.74 eV and -1.72 eV. In the $C_{24}H_{16}$ case, the four extra H atoms are bonded to C atoms on the edges. Consequently the aromatic skeleton is weakly perturbed and remains planar. In this case, the adsorption energy is close to the value obtained for coronene (Morisset et al., 2017). We have calculated interaction energies for more perturbed geometries (non planar with the aromatic skeleton curved), for example with the fourth H atom bonded to a C atom on the inner ring of the coronene molecule, facing either the vacuum or the graphene surface. The interaction energies are -1.46 eV and -1.64 eV, respectively. For $C_{24}H_{16}$, in the three configurations, planar, non planar with H facing the vacuum, non planar with H facing the graphene surface, interaction energies with the graphene are getting weaker and TPD peaks are located at lower temperatures (Skov et al., 2016; Morisset et al., 2017). When O atoms interact with hydrogenated coronene, the peaks corresponding to 304 and 305 masses are much less pronounced, as shown in the experiment coronene + H + O, figure 3a and 3b. Indeed, H atom abstraction reactions with O atoms are very efficient and superhydrogenated (+4H and +5H) coronene species are destroyed. However, for the 304 mass, the spectrum for coronene + H + O shows 2 peaks, one located at ∼410 K and the other one located at lower temperatures ∼330 K. The peak at ∼410 K, which is not observed in the coronene + H spectrum, can be assigned to planar (+4H on edges) species, in strong interaction with the

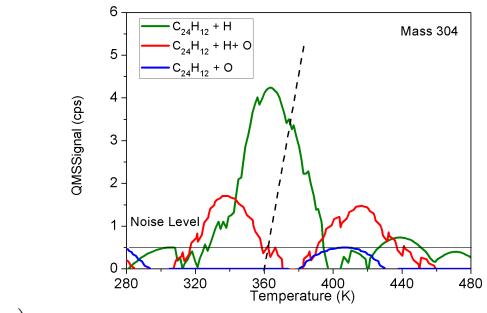

a)

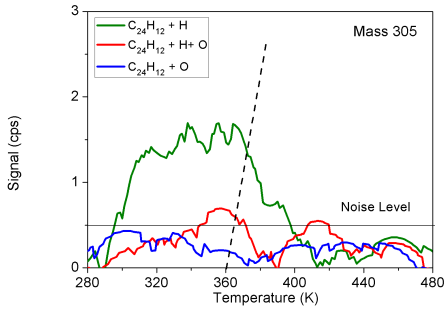

b)

Figure 3: TPD spectrum for mass 304 (a) and mass 305 (b). The dashed line represent the onset of the desorption of coronene.

surface, produced by abstraction of more superhydrogenated species (5H,6H,7H ...). The second peak at ∼330 K can be assigned to non planar hydrogenated species, in weaker interaction with the surface. One can notice that such species are observed in the coronene + H spectrum and remain in the coronene + H + O spectrum. Finally one could assign the intermediate TPD peak observed in the coronene + H experiment at ∼360 K to non planar super hydrogenated species, with H atom facing the vacuum side. Indeed, such species are expected to be efficiently abstracted by O atoms and the corresponding TPD peaks are expected to vanish in the coronene + H + O experiment. This highlights the fact that hydrogenated coronene species are highly reactive with O atoms. The last experiment, coronene + O, does not show peaks for masses 304 and 305 as expected.

4.3. Mass 316 : oxygenated coronene $C_{24}H_{12}O$

he spectra for mass 316 are reported in figure 4 for the 3 different experiments. Addition of oxygen on coronene molecules is observed in the coronene + H + O and coronene + O experiments. Considering the low exposure dose of O atoms (0.8 ML) and the relatively high temperature of the surface (50K), which implies fast O-desorption or O-recombination (Minissale et al., 2016), the coronene oxygenation is rather efficient and oxygenation cross sections are one order of magnitude higher than hydrogenation cross sections. The mass 316 TPD peaks observed in the coronene + H + O and coronene + O spectra are located at ∼420 K. This desorption temperature is slightly higher than the desorption temperature of coronene, as can be seen by comparing with the leading edge of the mass 300 curve. Therefore oxidised-coronene species are in strong interaction with the surface and associated geometries are planar or nearly planar. Peak intensities are comparable in the two spectra. Indeed, in the coronene + H + O experiment, considering the weak hydrogenation efficiency, most (∼ 70 %) of the coronene molecules are not hydrogenated, and same levels of detection of O-Coronene in coronene + H + O and coronene + O experiments are achieved. However the peak intensity in the coronene + H + O spectrum is smaller, this is probably related to the fact that O reactivity with hydrogenated PAH is high, and that a fraction of O atoms are consumed by abstraction reactions.

In gas phase DFT calculations, the addition of an O(^{3}P) atom on the coronene has been considered for two different types of sites: top sites and bridge sites (see figure 5). Addition energies of an O(^{3}P) atom on a coronene forming a triplet molecular state are reported for the different adsorption sites in table 1. The most stable species correspond to an O atom adsorbed on the edges of the coronene: on C atom in the outer edge position (T_1 site) and between two C atoms in outer edge position (B_1 site). O atom addition reactions on B_1 and T_1 sites are exoergic: $\triangle E_{addition} = -0.71$eV and -0.93 eV respectively, and associated barriers are: $E(TS_2) = 1.03$ eV and $E(TS_3) = 0.11$ eV, respectively, see figure 6 and table 2. In present experimental conditions, the O atom addition reaction is expected to proceed on T_1 sites.

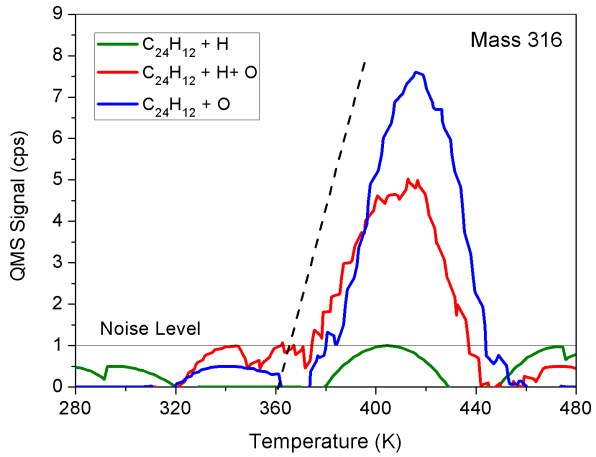

Figure 4: TPD spectrum for mass 300 in the 3 experiments. The leading edge of the mass 300 trace is represented by the dashed line.

For these two O-coronene species, the carbonaceous skeleton remains planar, and interaction with the surface is expected to be strong. Following our work on adsorption of hydrogenated coronenes on graphene (Morisset et al., 2017), we have performed DFT calculations on isolated oxygenated coronenes in a triplet state adsorbed on a graphene surface. The adsorption energies for the coronene oxygenated on the T1 site are -1.73 eV or -1.80 eV for species with the O atom oriented towards the graphene surface or towards the vacuum, respectively. These values are close to the adsorption energy of the coronene on the graphene surface: -1.74 eV. Consequently, desorption temperatures for T1 oxygenated coronene species are expected to be similar or slightly higher than the desorption temperature of the bare coronene. Experimentally, the desorption temperature for the mass 316 peak is slightly higher than the desorption temperatures of coronene (comparison with the leading edge of the mass 300 curve). Therefore, the calculations match very well with the experiments, and tend to show that desorbing $C_{24}H_{12}O$ species correspond to coronene molecules oxygenated on the edges.

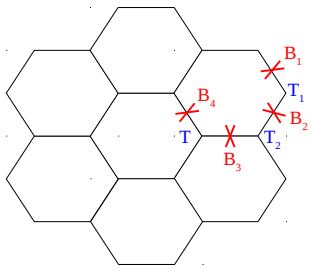

Figure 5: Oxygenation sites for the coronene. In blue : Top sites above a C atom. In red : sites in Bridge position

sites	$\triangle E_{addition}(eV)$
T_1	-0.93
T_2	-0.16
T	-0.01
B_1	-0.71
B_2	-0.43
B_3	> 0
B_4	> 0

Table 1: Addition energies of the O(^{3}P) atom on the coronene as function of sites (figure 5)

Starting from oxygenated coronene on T_1 site, we have considered, in DFT calculations, isomerization reactions corresponding to the migration of an H atom from the T_1 site to the adjacent ortho and para C atoms (I_4, I_2 and I_1 isomers figure 6) or to the O atom (I_3 isomer figure 6). The corresponding energies and transition states are presented in figure 6 and table 2:

- The I_4 isomer is the most stable (energy: -1.85 eV), but the associated transition state is high: E(TS_4) = 0.82 eV. This high barrier is related to an

important geometric perturbation of the adsorbent C atom upon isomerization.

- Isomers I_2 and I_3 have similar energies, -1.43 eV and -1.56 eV, respectively, but energies of the transition state differ: $E(TS_5) = 0.24$ eV and $E(TS_6) = 0.14$ eV, respectively. Indeed, the formation of the I_2 isomer, for which the H atom has migrated to the adjacent C inner edge site, involves a much more important geometric deformation than the formation of the I_3 isomer which corresponds to the alcohol in the triplet state.
- Isomer I_1, has the highest energy, -0.85 eV with $E(TS_7) = 0.22$ eV.

As discussed in the theoretical calculations section, the gas phase barriers calculated in the present work represent upper limits to the adsorbed phase values. Under the present experimental conditions, the mono-oxygenated coronene could correspond either to the top, I_1, I_2, or I_3 isomers.

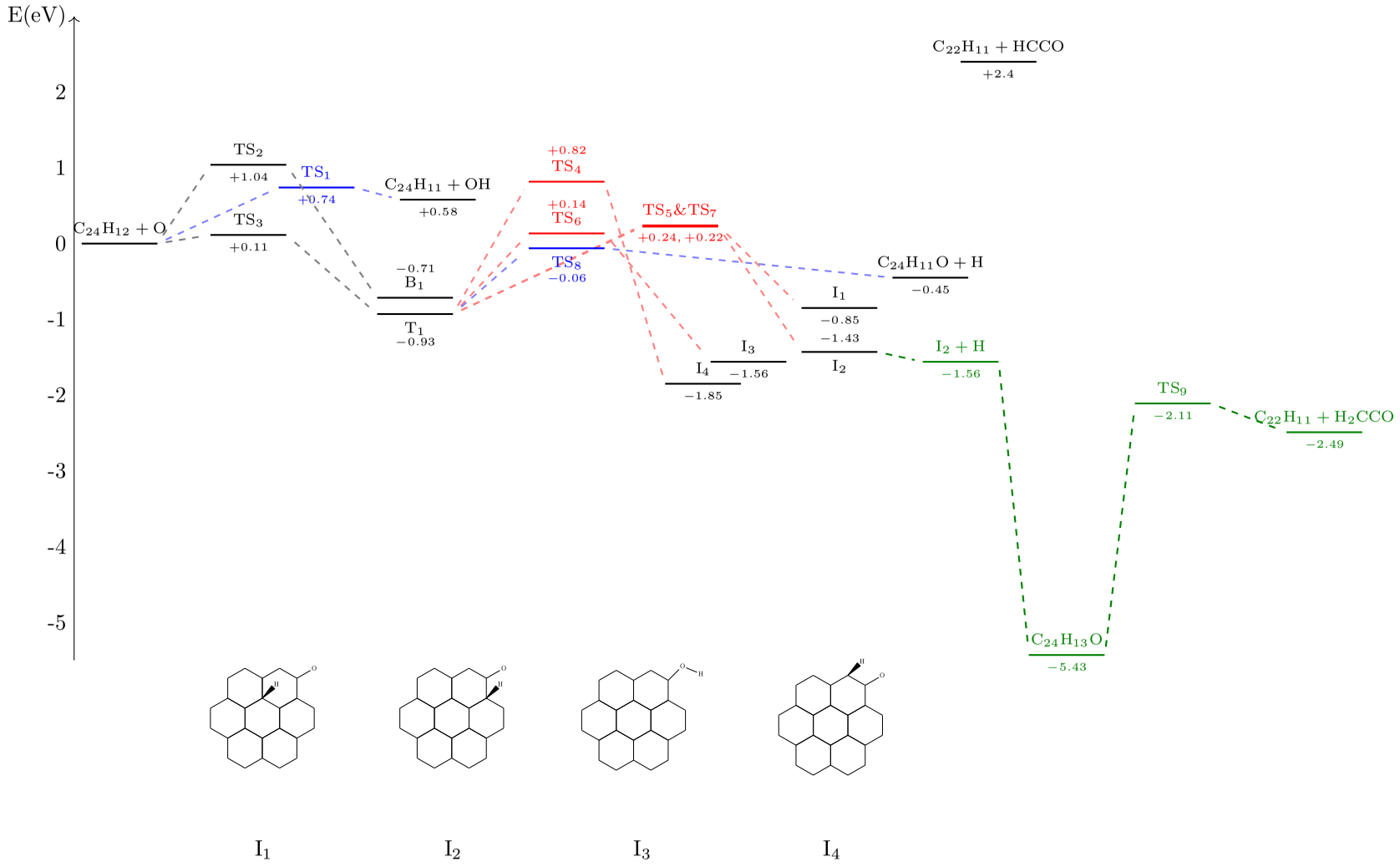

Figure 6: Schematic energy level diagram of the the reactions studied in present work, TS are the transition states, values are reported in table 2. In black : TS for O addition reactions ; blue : TS for abstraction or fragmentation reactions ; red : TS for isomerization reactions ; green : doublet states involved in hydrogenation and fragmentation of I_2. I_1 to I_4 : isomers of $C_{24}H_{12}O$.

4.4. Mass 275: fragmentation channels $C_{22}H_{11}$

In the coronene + O and coronene + H + O experiments, we have found that coronene related species were fragmenting in masses smaller than 300 amu. In order to study these fragmentations, we have systematically recorded masses between 270 and 300 amu. But due to the high number of masses to monitor, we have reduced the integration time for each of them. Therefore, for these fragmentation channels, the statistic and the temperature sampling are 4 times lower. The only positive detection of fragment occurs for the masses 275 and 277. In figure 7, the results for the mass 275 amu for the 3 experiments are reported. The methodology developed to assign positive detection is described as follow. We define two noise zones (stripped zones) before and after the central zone corresponding to the coronene desorption. In the central zone, both signal and noise are recorded. The number of events is compared in the two type of zones. For the experiments coronene + H and coronene + H + O, the signal is not statistically out of the noise whereas in the case of coronene + O, the detection of a mass 275 is clearly positive. As a matter of fact, in the experiment coronene + O, each reccord (except one) of the desorption zone shows at least one count.

In the experiment Coronene + O in figure 7, the average number of counts per reccord is about 4 counts. This value is close to the value of the half maximum peak in the TPD spectrum of mass 316 (see the figure 4), indicating that the efficiency of this fragmentation reaction and of the oxidation reaction are similar.

Therefore the experiment coronene + O shows an important fragmentation to the mass 275. This fragment is related to the loss of a second fragment of mass 41 and suggests a possible formation of HCCO following the oxygenation of the coronene molecules. However one has to determine whether this fragmentation is induced by the QMS detection (the mass 275 being a cracking pattern of O-Coronene), or if the fragment is formed on the surface. Careful examination of the desorption onset shows that O-coronene species desorb at higher temperatures than coronene, whereas fragments related to mass 275 desorb mainly at

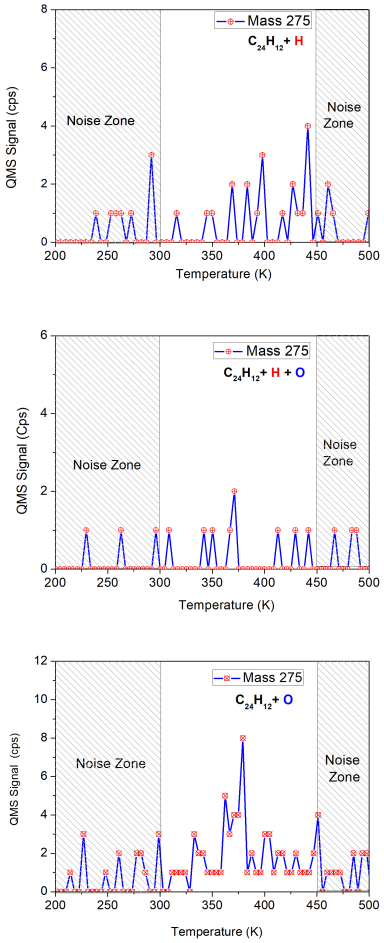

Figure 7: Scan of fragment masses: mass 275 is recorded with a sampling rate 4 times lower than previous curves shown, which have been smoothed by adjacent averaging. No averaging has been performed here, discrete counting is visible. The temperature below 300K is considered as a noise zone. The second noise zone is above 450 K, after the main desorption peaks. Mass 275 is doubtfully detected in experiment Coronene + H (top pannel), not detected in experiment Coronene + H + O (central pannel), and safely detected in experiment coronene + O

lower temperatures. Therefore we conclude that the fragmentation is due to the oxygenation, and not to the QMS detection.

In the gas phase DFT calculations, we have studied the direct abstraction and some fragmentation reactions.

The abstraction reaction $O(^3P) + C_{24}H_{12} \rightarrow OH + C_{24}H_{11}$ is endoergic ($\triangle E_{reaction} = 0.58$eV) and is associated to a high barrier ($E(TS_1) = 0.74$ eV), see figure 6 and table 2. In present experimental conditions, the OH formation (mass = 17) by direct abstraction is not expected to be observed.

The first considered fragmentation reaction, starting from the T_1 top species, corresponds to the H elimination: $C_{24}H_{12}O : T_1 \rightarrow C_{24}H_{11}O + H$. Indeed in the $O + C_2H_4$ (Fu et al., 2012), O + benzene (Boocock and Cvetanovic, 1961; Taatjes et al., 2010; Nguyen et al., 2007), and O + naphthalene (Scapinello et al., 2015) systems, H elimination reactions are prominent. Enhanced H atom lability has been also evidenced for O-coronene species produced after UV irradiation of coronene in water ice (Bernstein et al., 1999). With respect to the $C_{24}H_{12}+O(^3P)$ entrance channel, the energy of the products and the transition state are -0.45 eV and -0.06 eV, respectively (see figure 6 and table 2). In the present experimental conditions, this fragmentation channel is opened. Note that oxygenated $C_{24}H_{11}O$ molecules (mass 315) are not observed in the experiment. This could be related to further reactions (re hydrogenation or fragmentation). However, due to the presence of impurities in the coronene samples (methylated coronene), the mass 315 is a noisy reccord. Therefore this fragmentation pathway could occur experimentally.

The fragmentation reactions below, have been studied in order to explain the peak observed at mass 275. Starting from the I_2 isomer, the direct fragmentation reaction $C_{24}H_{12}O{:}I_2 \rightarrow C_{22}H_{11}+$ HCCO implies two C-C bond cleavages. The HCCO and $C_{22}H_{11}$ radicals correspond to mass 41 and 275, respectively. In our calculation, the energy of the products is high : +2.40 eV (see figure 6), therefore we conclude that this fragmentation cannot directly occur on the triplet potential energy surface. Since the direct fragmentation is not an opened channel, we have considered a fragmentation reaction involving hydrogenated/oxygenated

radical species $C_{24}H_{13}O$. Indeed, the I_2 isomer $C_{24}H_{12}O$ (figure 6) is a diradical, with a strong radical character on the C atom nearest to the O atom and located on the edge of the molecule. Hydrogenation of the I_2 isomer is exoergic : $\triangle E_{reaction}$ = -3.86 eV and barrierless. The H atoms could originate from $C_{24}H_{12}O : T_1 \rightarrow C_{24}H_{11}O + H$ reactions, or could also be transferred from the surface, as observed in the work of Thrower et al. (2014). In this study, it was experimentally shown that adsorbed coronene molecules can react with D-atoms pre-adsorbed on a graphite surface. The subsequent fragmentation reaction : $C_{24}H_{13}O \rightarrow C_{22}H_{11}O$ (mass=275) + H_2CCO (mass=42) is endoergic : $\triangle E = 2.93$ eV with a barrier with a negative energy (-2.11eV with respect to the energy origin $C_{24}H_{12}$+O, see figure 6 and table 2). In present experimental conditions, this fragmentation channel is opened and could explain the observation of the mass 275 and may be a route for the ketene formation. However, these theoretical results were obtained after the experiment was stopped and mass 42 was not measured.

4.5. Mass ratios relative to parent mass

The figure 8 shows a comparison of the different chemical channels for the different experimental conditions. The coronene experiment only shows the mass 300, as expected. The coronene + H experiments demonstrate through the presence of mass 304 and 305 that in our experimental conditions a moderate degree of hydrogenation is achieved. The coronene + H + O experiments demonstrate that hydrogenated coronene are highly reactive with O atoms. Actually the mass 304 and 305 become almost undetectable or very reduced when O atoms interact with hydrogenated PAH. The most probable mechanism is abstraction (PAH-H+O $\longrightarrow$ PAH+OH) since neither mass 317 nor specific fragmentations are detected. The observation of the mass 316, in a relative high abundance, demonstrates that the barrier to the O-addition on coronene is crossed in present experimental conditions. In a very rough approximation, one can estimate that the kinetics of the O addition reaction and of the O-diffusion and desorption

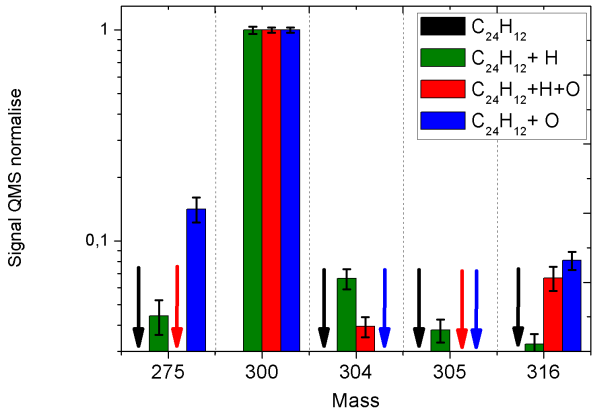

Figure 8: Mass ratio relative to mass 300 of the coronene (in black), coronene + H (in red), coronene + H + O (in blue) and the coronene + O measurements (in green). Arrows are plotted where the values are lower than 0.03, which corresponds approximately to uncertainty level. Error bars represent statistical fluctuations.

processes are in competition. One can infer that the O-addition should be faster than the O recombination, otherwise, most of O atoms would be consumed in an unobservable channel corresponding to the desorption of O_2. In the case of a reaction faster than the diffusion mechanism and assuming the values obtained in Minissale et al. (2016) (i.e. 750 K for diffusion and 1420 K for desorption), we find a typical lower boundary value of 40 meV for the barrier to the reaction PAH+O $\longrightarrow$ PAH-O. For the upper limit, if the reaction rate is limited by the desorption rate of O atoms, the barrier to reaction should be smaller than the adsorption energy of O atoms on the surface and should be about or lower than 110 meV. This is in line with our theoretical calculations.

Finally, in the experiment PAH + O, the mass 275 is of the same order of magnitude as the mass 316, indicating that the fragmentation is an important channel of the oxidation of PAHs.

Reactions	type	TS	$E(eV)$	$E_{Products}$ (eV)
$C_{24}H_{12} + O \rightarrow C_{24}H_{11} + OH$	H abstraction	TS1	0.74	0.58
$C_{24}H_{12} + O \rightarrow C_{24}H_{12}O : B_1$	O addition	TS2	1.03	−0.71
$C_{24}H_{12} + O \rightarrow C_{24}H_{12}O : T_1$	O addition	TS3	0.11	−0.93
$C_{24}H_{12}O : T_1 \rightarrow I_4$	isomerization	TS4	0.82	−1.85
$C_{24}H_{12}O : T_1 \rightarrow I_2$	isomerization	TS5	0.24	−1.43
$C_{24}H_{12}O : T_1 \rightarrow I_3$	isomerization	TS6	0.14	−1.56
$C_{24}H_{12}O : T_1 \rightarrow I_1$	isomerization	TS7	0.22	−0.85
$C_{24}H_{12}O : T_1 \rightarrow C_{24}H_{11}O + H$	fragmentation	TS8	−0.06	−0.45
$C_{24}H_{12}O : I_2 + H \rightarrow C_{24}H_{13}O$	hydrogenation	no	–	−3.86
$C_{24}H_{13}O \rightarrow C_{22}H_{11} + H_2CCO$	fragmentation	TS9	−2.11	−2.49
$C_{24}H_{12}O : I_2 \rightarrow C_{22}H_{11} + HCCO$	fragmentation	nc	–	2.40

Table 2: Energies of the transition states (TS) and products for reactions reported in figure 6, zero energy level: $C_{24}H_{12}$ + O(^{3}P). nc : not calculated.

5. Astrophysical applications

Our combined experimental and theoretical results indicate that oxygenation of coronene leads to either oxygenation ($C_{24}H_{12}O$) or H loss of the coronene molecules. In a second step, hydrogen addition to the oxygenated coronene can lead to the fragmentation of the molecule and H_2CCO loss. The formation of molecules such as H_2CCO and HCCO has been debated in the literature (Occhiogrosso et al. 2013). It has been proposed that oxygenation of unsaturated hydrocarbons easily breaks their multiple C-C bounds to form HCCO or HCO, which are precursors of CO. In this later study, small unsaturated hydrocarbons are considered (such as C_2H_4, C_2H_2, CH_3CCH, CH_2CCH_2), with reactions rates based on laboratory studies (Capozza et al. 2004; Fu et al.).

The recent detection of HCCO and H_2CCO in cold environments (Agúndez et al. 2015) raised many questions on the origin of these molecules. Indeed, observations report the detection of HCCO toward the starless core Lupus-1A and the molecular cloud L483, with abundances of 10^{-11} relative to H_2 (Agúndez

et al. 2015). H_2CCO has also been detected in these two regions, and is $\sim$ 10 times more abundant than HCCO. Because of the low temperatures in these environments, the presence of HCCO cannot be explained by gas phase reactions and its calculated abundance remains 6 orders of magnitude below that calculated for H_2CCO (Occhiogrosso et al. (2013)). An alternative formation route has been proposed (Wakelam et al., 2015) where reactions on dust would allow solid CCO to react with H atoms to form efficiently HCCO (Wakelam et al., 2015). Since this reaction is exothermic, chemical desorption could account for its release into the gas phase. This formation route does reproduce the abundances (density of HCCO relative to H_2) of HCCO in dark clouds.

H_2CCO has been observed in different PDRs with large (Orion bar and Mon R2 with χ= 10^4–10^5) and weaker UV radiation fields (Horsehead with χ=60). In the Orion bar, Cuadrado et al. (2017) detected H_2CCO and derived a abundance of 0.9 $10\times$ 10^{-10} (density relative to H_2) . In Mon R2, H_2CCO has also been detected (Trevio-Morales et al. in prep). In the Horsehead PDR, H_2CCO has been detected, with abundances relative to H_2 3 times higher in the PDR than in the core (Guzmán et al., 2014). However, HCCO has not been detected in these PDRs. In these PDRs nevertheless, PAHs have been detected (Peeters et al. (2002) for Orion Bar, Berné et al. (2009) for Mon R2 and Compiègne et al. (2007) for Horsehead).

From the calculations performed in this study, the fragmentation of coronene molecules can occur via the isomer I2 after a coronene reacted with an O(^{3}P), as shown in Fig.6. Coronene reacts with an O(^{3}P) and oxygen is attached in top site. This oxygenated coronene is reached with a transition state TS1 of 0.11 eV. It can then reach the isomer I2 via a transition state TS5 of 0.24 eV. Hydrogenation of the I2 isomer leads to the fragmentation of coronene and the formation of H_2CCO. Considering the oxygenation of PAHs, the rate can be written as R_O=n_O $\times v(O) \times n_{PAH}\sigma_{PAH} \times \exp -\frac{E_f}{Tgas}$, where n_O is the density of oxygen atoms, assumed to be 10^{-4} n_H, $v(O)$ is the the thermal velocity of oxygens $\frac{10^5}{\sqrt{m_O}}\sqrt{\frac{T_{gas}}{100}}$ cm s^{-1} , σ the cross section for the reaction, taken as 1.6 $\mathring{A}^2$ (as in Mennella et al. (2012) for hydrogenation), n_{PAH} is the density of

PAHs, taken as 10^{-7}n$_H$ and E$_f$ is the largest barrier involved in the successive reactions leading to the fragmentation in H_2CCO. The rate for oxygenation leading to fragmentation is then, R$_O$=9.6 10^{-24} n$_H^2\sqrt{(Tgas)}$ exp$(-\frac{E_f}{T_{gas}})$ s^{-1}. Others rates, if required, such as H accretion are not limiting rates.

For warm PDRs with T$_{gas}$ $\sim$ 300K, it takes only few hundreds of years for the PAHs to react with oxygen, following a path to fragmentation. This is a very short time in the life time of a cloud. At 100 K however, this time becomes $\sim 10^9$ years. Therefore, the fragmentation route proposed in this study where a PAH fragment in H_2CCO can be easily reached in warm PDRs on very short timescales.

6. Conclusion

In this work, we have studied the reactivity of O(^{3}P) atoms with coronene molecules deposited on a graphite surface. Experimentally, the coronene + H, coronene + O and coronene + H + O systems have been considered. The main results are that the oxygenation of coronene is more effective than hydrogenation and leads to significant fragmentations. In support of these results, DFT calculations on the system coronene + O(^{3}P) were performed. One of the main results is that O atoms can adsorb on the edges of coronene molecules with a small barrier (0.11 eV, i.e. $\sim$ 1275 K). Our calculations have shown that the direct fragmentation reactions, leading to HCCO molecules, are not energetically favorable for the triplet state. In addition, we have proposed a fragmentation scheme, involving the hydrogenation of $C_{24}H_{12}O$ molecules, that can lead to the formation of H_2CCO. This fragmentation scheme is energetically favorable. By estimating the reaction rates of PAHs with oxygen in the MIS, we can conclude that the oxidation barrier is low enough so that, in a 300 K gas, oxidation of PAHs become a destructive pathway to be taken into account, and a potential source of ketene or even ketenyl.

References

ADF2017, 2017. SCM Theoretical Chemistry Vrije Universiteit, Amsterdam The Netherlands http://www.scm.com. .

Agúndez, M., Cernicharo, J., Guélin, M., 2015. Discovery of interstellar ketenyl (HCCO), a surprisingly abundant radical. Astron. Astrophys. 577, L5. doi:10.1051/0004-6361/201526317, arXiv:1504.05721.

Allamandola, L.J., Tielens, A.G.G.M., Barker, J.R., 1985. Polycyclic aromatic hydrocarbons and the unidentified infrared emission bands - Auto exhaust along the Milky Way. 290, L25–L28. doi:10.1086/184435.

Allamandola, L.J., Tielens, A.G.G.M., Barker, J.R., 1989. Interstellar polycyclic aromatic hydrocarbons - The infrared emission bands, the excitation/emission mechanism, and the astrophysical implications. 71, 733–775. doi:10.1086/191396.

Andrews, H., Candian, A., Tielens, A.G.G.M., 2016. Hydrogenation and dehydrogenation of interstellar PAHs: Spectral characteristics and H_2 formation. Astron. Astrophys. 595, A23. doi:10.1051/0004-6361/201628819.

Appel, J., Bockhorn, H., Frenklach, M., 2000. Kinetic modeling of soot formation with detailed chemistry and physics: laminar premixed flames of C2 hydrocarbons. Combust. Flame 12, 122.

Barckholtz, C., Barckholtz, T.A., Hadad, C.M., 2001. A Mechanistic Study of the Reactions of H, O(^{3}P), and OH with Monocyclic Aromatic Hydrocarbons by Density Functional Theory. J. Phys. Chem. A 105, 140–152.

Berné, O., Fuente, A., Goicoechea, J.R., Pilleri, P., González-García, M., Joblin, C., 2009. Mid-Infrared Polycyclic Aromatic Hydrocarbon and H_2 Emission as a Probe of Physical Conditions in Extreme Photodissociation Regions. 706, L160–L163. doi:10.1088/0004-637X/706/1/L160, arXiv:0910.3935.

Berné, O., Joblin, C., Deville, Y., Smith, J.D., Rapacioli, M., Bernard, J.P., Thomas, J., Reach, W., Abergel, A., 2007. Analysis of the emission of very small dust particles from Spitzer spectro-imagery data using blind signal separation methods. Astron. Astrophys. 469, 575–586. doi:10.1051/0004-6361:20066282, arXiv:astro-ph/0703072.

Bernstein, M.P., Moore, M.H., Elsila, J.E., Sandford, S.A., Allamandola, L.J., Zare, R.N., 2002. Side group addition to the polycyclic aromatic hydrocarbon coronene by proton irradiation in cosmic ice analogs. The Astrophysical Journal 582, L25–L29. URL: https://doi.org/10.1086%2F345941, doi:10.1086/345941.

Bernstein, M.P., Sandford, S.A., Allamandola, L.J., Gilette, J.S., Clemett, S.J., Zare, R.N., 1999. UV Irradiation of Polyclyclic Aromatic Hydrocarbons in Ices: Production of Alcohols, Quinones and Ethers. Science 283, 1135–1138.

Boocock, G., Cvetanovic, R., 1961. Canadian J. Chem. 39, 2436.

Boschman, L., Reitsma, G., Cazaux, S., Schlathölter, T., Hoekstra, R., Spaans, M., González-Magaña, O., 2012. Hydrogenation of PAH cations: a first step toward H_2 formation. Astrophys. J. 761, L33. URL: http://iopscience.iop.org.ezproxy.obspm.fr/article/10.1088/2041-8205/761/2/L33, doi:10.1088/2041-8205/761/2/L33.

Bouwman, J., Mattioda, A.L., Linnartz, H., Allamandola, L.J., 2011. Photochemistry of polycyclic aromatic hydrocarbons in cosmic water ice. Astronomy & Astrophysics 525, A93. URL: http://www.aanda.org/10.1051/0004-6361/201015059, doi:10.1051/0004-6361/201015059.

Capozza, G., Segoloni, E., Leonori, F., Volpi, G.G., Casavecchia, P., 2004. Soft electron impact ionization in crossed molecular beam reactive scattering: The dynamics of the $O(^3P)+C_2H_2$ reaction. J. Chem. Phys. 120, 4557–4560. doi:10.1063/1.1652013.

Castellanos, P., Candian, A., Andrews, H., Tielens, A.G.G.M., 2018. Photoinduced polycyclic aromatic hydrocarbon dehydrogenation. Molecular hydrogen formation in dense PDRs. Astron. Astrophys. 616, A167. doi:10.1051/0004-6361/201833221, arXiv:1806.02708.

Cazaux, S., Minissale, M., Dulieu, F., Hocuk, S., 2016. Dust as interstellar catalyst. II. How chemical desorption impacts the gas. Astron. Astrophys. 585, A55. doi:10.1051/0004-6361/201527187, arXiv:1511.02461.

Cazaux, S., Morisset, S., Spaans, M., Allouche, A., 2011. When sticking influences H_2 formation. Astron. Astrophys. 535, A27. URL: http://www.aanda.org/10.1051/0004-6361/201117220, doi:10.1051/0004-6361/201117220.

Cazaux, S., Tielens, A.G.G.M., 2004. H_2 Formation on Grain Surfaces. Astron. Astrophys. 604, 222–237. doi:10.1086/381775.

Chaabouni, H., Bergeron, H., Baouche, S., Dulieu, F., Matar, E., Congiu, E., Gavilan, L., Lemaire, J.L., 2012. Sticking coefficient of hydrogen and deuterium on silicates under interstellar conditions. Astron. Astrophys. 538, A128. URL: http://www.aanda.org/articles/aa/full{_}html/2012/02/aa17409-11/aa17409-11.html, doi:10.1051/0004-6361/201117409.

Compiègne, M., Abergel, A., Verstraete, L., Reach, W.T., Habart, E., Smith, J.D., Boulanger, F., Joblin, C., 2007. Aromatic emission from the ionised mane of the Horsehead nebula. Astron. Astrophys. 471, 205–212. doi:10.1051/0004-6361:20066172, arXiv:0706.1510.

Congiu, E., Chaabouni, H., Laffon, C., Parent, P., Baouche, S., Dulieu, F., 2012. Efficient surface formation route of interstellar hydroxylamine through NO hydrogenation. I. The submonolayer regime on interstellar relevant substrates. J. Chem. Phys. 137, 054713. URL: http://scitation.aip.org.ezproxy.obspm.fr/content/aip/journal/jcp/137/5/10.1063/1.4738895, doi:10.1063/1.4738895.

Cook, A.M., Ricca, A., Mattioda, A.L., Bouwman, J., Roser, J., Linnartz, H., Bregman, J., Allamandola, L.J., 2015. Photochemistry of Polycyclic Aromatic Hydrocarbons in Cosmic Water Ice: The Role of PAH Ionization and Concentration. 799, 14. doi:10.1088/0004-637X/799/1/14.

Cuadrado, S., Goicoechea, J.R., Cernicharo, J., Fuente, A., Pety, J., Tercero, B., 2017. Complex organic molecules in strongly UV-irradiated gas. Astron. Astrophys 603, A124. doi:10.1051/0004-6361/201730459, arXiv:1705.06612.

Cuylle, S.H., Allamandola, L.J., Linnartz, H., 2014. Photochemistry of PAHs in cosmic water ice. The effect of concentration on UV-VIS spectroscopy and ionization efficiency. 562, A22. doi:10.1051/0004-6361/201322495.

de Barros, A.L.F., Mattioda, A.L., Ricca, A., Cruz-Diaz, G.A., Allamandola, L.J., 2017. Photochemistry of Coronene in Cosmic Water Ice Analogs at Different Concentrations. 848, 112. doi:10.3847/1538-4357/aa8c71.

Fu, B., Han, Y.C., Bowman, J., Angelucci, L., Balucani, N., Leonori, F., Casavecchia, P., 2012. Proc. Natl. Acad. Sci. USA 109, 9733.

Fu, B., Han, Y.C., Bowman, J.M., Angelucci, L., Balucani, N., Leonori, F., Casavecchia, P., .

Goulay, F., Rebrion-Rowe, C., Le Garrec, J.L., Le Picard, S.D., Canosa, A., Rowe, B.R., 2005. The reaction of anthracene with oh radicals: An experimental study of the kinetics between 58 and 470k. The Journal of Chemical Physics 122, 104308. URL: https://doi.org/10.1063/1.1857474, doi:10.1063/1.1857474, arXiv:https://doi.org/10.1063/1.1857474.

Gudipati, M.S., Allamandola, L.J., 2003. Facile generation and storage of polycyclic aromatic hydrocarbon ions in astrophysical ices. The Astrophysical Journal 596, L195–L198. URL: https://doi.org/10.1086%2F379595, doi:10.1086/379595.

Gudipati, M.S., Allamandola, L.J., 2006. Unusual Stability of Polycyclic Aromatic Hydrocarbon Radical Cations in Amorphous Water Ices up to 120 K: Astronomical Implications. 638, 286–292. doi:10.1086/498816.

Guennoun, Z., Aupetit, C., Mascetti, J., 2010. Photochemistry of coronene with water at 10K: first tentative identification by infrared spectroscopy of oxygen containing coronene products. Phys. Chem. Chem. Phys. 13, 7340–7347.

Guzmán, V.V., Pety, J., Gratier, P., Goicoechea, J.R., Gerin, M., Roueff, E., Le Petit, F., Le Bourlot, J., 2014. Chemical complexity in the Horsehead photodissociation region. Faraday Discussions 168, 103–127. doi:10.1039/C3FD00114H, arXiv:1404.7798.

Habart, E., Boulanger, F., Verstraete, L., Walmsley, C.M., Pineau des Forêts, G., 2004. Some empirical estimates of the H_2 formation rate in photon-dominated regions. Astron. Astrophys. 414, 531–544. doi:10.1051/0004-6361:20031659, arXiv:arXiv:astro-ph/0311040.

Hirama, M., Tokosumi, T., Ishida, T., ichi Aihara, J., 2004. Possible molecular hydrogen formation mediated by the inner and outer carbon atoms of typical pah cations. Chemical Physics 305, 307 – 316. URL: http://www.sciencedirect.com/science/article/pii/S0301010404003714, doi:10.1016/j.chemphys.2004.07.010.

Hollenbach, D., Kaufman, M.J., Bergin, E.A., Melnick, G.J., 2009. Water, O_2, and Ice in Molecular Clouds. Astrophys. J. 690, 1497–1521. doi:10.1088/0004-637X/690/2/1497, arXiv:0809.1642.

Jensen, P.A., Leccese, M., Simonsen, F.D.S., Skov, A.W., Bonfanti, M., Thrower, J.D., Martinazzo, R., Hornekær, L., 2019. Identification of stable configurations in the superhydrogenation sequence of polycyclic aromatic hydrocarbon molecules. Monthly Notices of the Royal Astronomical Society 486, 5492–5498. URL: https://academic.oup.com/mnras/article/486/4/5492/5484867, doi:10.1093/mnras/stz1202.

Jones, A.P., Fanciullo, L., Köhler, M., Verstraete, L., Guillet, V., Bocchio, M., Ysard, N., 2013. The evolution of amorphous hydrocarbons in the ISM: dust modelling from a new vantage point. Astron. Astrophys. 558, A62. doi:10.1051/0004-6361/201321686, arXiv:1411.6293.

Köhler, M., Ysard, N., Jones, A.P., 2015. Dust evolution in the transition towards the denser ISM: impact on dust temperature, opacity, and spectral index. 579, A15. doi:10.1051/0004-6361/201525646, arXiv:1506.01533.

Leger, A., Puget, J.L., 1984. Identification of the 'unidentified' IR emission features of interstellar dust? 137, L5–L8.

Lynch, B., Fast, P., Harris, M., Truhlar, D.G., 2000. J. Phys. Chem. A 104, 4811.

Mennella, V., Hornekær, L., Thrower, J., Accolla, M., 2012. The Catalytic Role of Coronene for Molecular Hydrogen Formation. 745, L2. doi:10.1088/2041-8205/745/1/L2.

Minissale, M., Congiu, E., Dulieu, F., 2016. Direct measurement of desorption and diffusion energies of O and N atoms physisorbed on amorphous surfaces. Astron. Astrophys. 585, A146. URL: http://cdsads.u-strasbg.fr/abs/2016A{%}26A...585A.146M, doi:10.1051/0004-6361/201526702.

Morisset, S., Rougeau, N., Teillet-Billy, D., 2017. Chem. Phys. Lett. 679, 225.

Nguyen, T., Talbi, D., Congiu, E., Baouche, S., Karton, A., Loison, J.C., Dulieu, F., 2019. Experimental and Theoretical Study of the Chemical Network of the Hydrogenation of NO on Interstellar Dust Grains. ACS Earth and Space Chemistry 3, 1196–1207. URL: http://pubs.acs.org/doi/10.1021/acsearthspacechem.9b00063, doi:10.1021/acsearthspacechem.9b00063.

Nguyen, T.L., Peeters, J., Vereecken, L., 2007. Theoretical reinvestigation of the O(^{3}P) + C_6H_6 Reaction: Quantum Chemical and Statistical Rate Calculations. J. Phys. Chem. A 111, 3836–3849.

Noble, J.A., Jouvet, C., Aupetit, C., Moudens, A., Mascetti, J., 2017. Efficient photochemistry of coronene:water complexes. 599, A124. doi:10.1051/0004-6361/201629613, arXiv:1612.03008.

Occhiogrosso, A., Viti, S., Balucani, N., 2013. An improved chemical scheme for the reactions of atomic oxygen and simple unsaturated hydrocarbons - implications for star-forming regions. Mon. Not. R. Astron. Soc 432, 3423–3430. doi:10.1093/mnras/stt694, arXiv:1304.5899.

Peeters, E., Hony, S., Van Kerckhoven, C., Tielens, A.G.G.M., Allamandola, L.J., Hudgins, D.M., Bauschlicher, C.W., 2002. The rich 6 to 9 μm spectrum of interstellar PAHs. Astron. Astrophys. 390, 1089–1113. doi:10.1051/0004-6361:20020773, arXiv:astro-ph/0205400.

Pilleri, P., Joblin, C., Boulanger, F., Onaka, T., 2015. Mixed aliphatic and aromatic composition of evaporating very small grains in NGC 7023 revealed by the 3.4/3.3 μm ratio. Astron. Astrophys. 577, A16. doi:10.1051/0004-6361/201425590, arXiv:1502.04941.

Rapacioli, M., Joblin, C., Boissel, P., 2005. Spectroscopy of polycyclic aromatic hydrocarbons and very small grains in photodissociation regions. Astron. Astrophys. 429, 193–204. doi:10.1051/0004-6361:20041247.

Ricca, A., Bauschlicher, Charles W., J., 2000. The reactions of polycyclic aromatic hydrocarbons with OH. Chemical Physics Letters 328, 396–402. doi:10.1016/S0009-2614(00)00915-5.

Scapinello, M., Martini, L.M., Tosi, P., Maranzana, A., Tonachini, G., 2015. Molecular growth of PAH-like systems induced by oxygen species: experimental and theoretical study of the reaction of naphthalene with HO, O and O_2. RSC Adv. 5, 38581.

Skov, A.W., Andersen, M., Thrower, J.D., Jørgensen, B., Hammer, B., Hornekær, L., 2016. The influence of coronene super-hydrogenation on the

coronene-graphite interaction. J. Chem. Phys. 145, 174708. doi:10.1063/1.4966259.

Taatjes, C.A., Osborn, D.L., Selby, T.M., Meloni, G., Trevitt, A.J., Epifanovsky, E., Krylov, A.I., Sirjean, B., Dames, E., Wang, H., 2010. Products of the Benzene + O (^{3}P) Reaction. J. Phys. Chem. A 114, 3355–3370.

te Velde, G., Bickelhaupt, F., Baerends, E., Fonseca Guerra, C., van Gisbergen, S., Snijders, J., Ziegler, T., 2001. J. Comput. Chem. 22, 931.

Thrower, J.D., Friis, E.E., Skov, A.L., Jørgensen, B., Hornekær, L., 2014. Hydrogenation of PAH molecules through interaction with hydrogenated carbonaceous grains. Phys. Chem. Chem. Phys. 16, 3381–7. URL: http://pubs.rsc.org.ezproxy.obspm.fr/en/content/articlehtml/2014/cp/c3cp54073a, doi:10.1039/c3cp54073a.

Thrower, J.D., Jørgensen, B., Friis, E.E., Baouche, S., Mennella, V., Luntz, A.C., Andersen, M., Hammer, B., Hornekær, L., 2012. Experimental evidence for the formation of highly superhydrogenated polycyclic aromatic hydrocarbons through H atom addition and their catalytic role in H_2 formation. Astrophys. J. 752, 3. URL: http://iopscience.iop.org.ezproxy.obspm.fr/article/10.1088/0004-637X/752/1/3, doi:10.1088/0004-637X/752/1/3.

Tielens, A.G.G.M., 2013. The molecular universe. Rev. Mod. Phys. 85, 1021–1081. URL: https://link.aps.org/doi/10.1103/RevModPhys.85.1021, doi:10.1103/RevModPhys.85.1021.

Ulbricht, H., Moos, G., Hertel, T., 2002. Physisorption of molecular oxygen on single-wall carbon nanotube bundles and graphite. Phys. Rev. B 66, 075404. URL: https://link.aps.org/doi/10.1103/PhysRevB.66.075404, doi:10.1103/PhysRevB.66.075404.

Wakelam, V., Bron, E., Cazaux, S., Dulieu, F., Gry, C., Guillard, P., Habart, E., Hornekær, L., Morisset, S., Nyman, G., Pirronello, V., Price, S.D., Valdivia, V., Vidali, G., Watanabe, N., 2017. H_2 formation on interstellar dust grains:

The viewpoints of theory, experiments, models and observations. Mol. Astrophys. 9, 1–36. URL: https://www.sciencedirect.com/science/article/pii/S2405675817300271?via{%}3Dihub, doi:10.1016/J.MOLAP.2017.11.001.

Wakelam, V., Loison, J.C., Hickson, K.M., Ruaud, M., 2015. A proposed chemical scheme for HCCO formation in cold dense clouds. Mon. Not. R. Astron. Soc 453, L48–L52. doi:10.1093/mnrasl/slv097, arXiv:1509.00336.

Wang, H., Frenklach, M., 1997. A detailed kinetic modeling study of aromatics formation in laminar premixed acetylene and ethylene flames. Combust. Flame 110, 173.

Ward, M.D., Price, S.D., 2011. Astrophys. J. 741, 121.

Weingartner, J.C., Draine, B.T., 2001. Dust Grain-Size Distributions and Extinction in the Milky Way, Large Magellanic Cloud, and Small Magellanic Cloud. Astrophys. J. 548, 296–309. doi:10.1086/318651, arXiv:arXiv:astro-ph/0008146.

Whittet, D.C.B., Gerakines, P.A., Hough, J.H., Shenoy, S.S., 2001. Interstellar Extinction and Polarization in the Taurus Dark Clouds: The Optical Properties of Dust near the Diffuse/Dense Cloud Interface. Astrophys. J. 547, 872–884. doi:10.1086/318421.